098640

Available online at www.sciencedirect.com
SCIENCE DIRECT
ELSEVIER
Journal of Contaminant Hydrology 60 (2003) 135–162
JOURNAL OF Contaminant Hydrology
www.elsevier.com/locate/jconhyd

Harmonic analysis of flow in open boreholes due to barometric pressure cycles

Donald A. Neeper *

Science and Engineering Associates, Inc., 3205 Richards Lane, Suite A, Santa Fe, NM 87505, USA

Received 28 June 2001; received in revised form 12 July 2002; accepted 24 July 2002

Abstract

Barometric pressure changes can induce airflow in an open borehole or well screened in the vadose zone, thereby ventilating the soil surrounding the borehole. This paper presents an analytic model of the induced airflow and compares the predictions of the model with experimental measurements. This model may be useful for the design of passive soil vapor extraction as applied to the remediation of soil contaminated by volatile organic compounds (VOCs). Based on harmonic analysis, the model predicts the time-dependent flow in agreement with measurements at a borehole in strata of differing permeability. The model uses no adjustable parameters, but proceeds from first principles based upon known or estimated values of soil properties as a function of depth. In an approximation, the calculated flow is determined by the difference between barometric pressure and the attenuated pressure that would propagate vertically into the vadose zone in the absence of an open borehole. The attenuated vertical propagation of pressure can be calculated by a corresponding harmonic method presented previously. The model reveals that the flow in the borehole is approximately proportional to the horizontal permeability in the formation, and depends only weakly on the soil porosity and borehole radius.
© 2002 Elsevier Science B.V. All rights reserved.

Keywords: Soil vapor extraction; Atmospheric pressure; Vadose zone; Harmonic analysis; Barometric pumping

* WGI/PMC/SEA Los Alamos Project Office, 2237 Trinity Dr. Bldg. 2, Los Alamos, NM 87544, USA. Fax: +1-505-662-1398.
E-mail address: dneeper@aol.com (D.A. Neeper).

0169-7722/02/$ - see front matter © 2002 Elsevier Science B.V. All rights reserved.
PII: S0169-7722(02)00086-4

30853

1. Introduction

1.1. Active and passive soil vapor extraction

Soil vapor extraction (SVE) is an established technology for remediation of soils contaminated by volatile chemicals (Pedersen and Curtis, 1991; Michaels, 1996; DiGiulio, 1996). In active SVE, vapors are swept from the subsurface by a vacuum pump connected to a well screened in the contaminated region of the vadose zone. Numerous analytic and numerical modeling efforts have addressed the subsurface air motion as determined by the configuration of the extraction well, soil permeability, and other parameters. See, for example, Wilson et al. (1988), Johnson et al. (1990), Johnson and Ettinger (1994), Baehr and Joss (1995), and Massmann et al. (2000).

In passive soil vapor extraction, the extraction well is connected to the atmosphere so that subsurface airflow to and/or from the well is induced by barometric variations. Passive SVE proceeds more slowly than active extraction, but it requires minimal maintenance and needs no rotating machinery. It is especially applicable to sites that do not require rapid removal of contaminants, or sites where long-term oxygenation of the soil is needed for bioremediation, sometimes called "bioventing." Ellerd et al. (1999) provide a review of passive SVE. Foor et al. (1995) review passive bioventing. Fig. 1 illustrates passive ventilation, in which radial flow to and from the well is affected not only by the barometric pressure variation in the well itself, but also by the delayed and attenuated pressure variations that penetrate the ground vertically. At any particular depth and time, air will

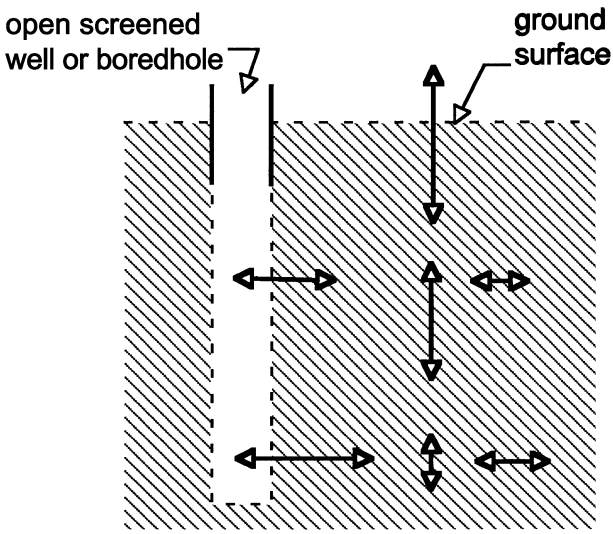

Fig. 1. Schematic diagram depicting vertical flow from ground surface and radial flow from an open screened well or borehole.

flow radially through the borehole wall or well screen if the pore pressure in the surrounding formation differs from the current atmospheric pressure in the well.

Small pressure variations in porous media propagate according to the diffusion equation, for which one-dimensional harmonic solutions are available for either planar propagation from ground surface or radial propagation from an open cylindrical borehole. Therefore, this article presents an algebraic model of flow based on harmonic analysis, taking approximate account of both the vertical and radial propagation. Given the permeability and porosity as functions of depth, the model successfully represents the measured flows using no adjustable parameters. It is expected that a subsequent report will examine the relationship between the measured extraction rate of vapors and the varying volume flow rate, wherein the oscillating radial flow near the borehole may locally influence the vapor transport (Neeper, 2001, hereinafter referred to as {I}). If the porosity and vertical permeability are known, the vertical propagation of pressure can be calculated by the planar harmonic analysis presented earlier (Neeper, 2002, hereinafter referred to as {II}). The equations presented in {II} and those presented here can be programmed for computer solution, comprising tools for estimating the flow in passive SVE systems. Appendix B illustrates programming of the radial flow equations presented here.

1.2. Application of passive soil vapor extraction

In many cases of active SVE, the concentration of the contaminant vapors in the effluent gas decreases asymptotically to a small non-zero value, necessitating the continuation of extraction for months or years. This so-called "tailing" of the effluent concentration is attributed to various rate processes in which sorbed or dissolved phases of the contaminant gradually evaporate and migrate as vapor to channels in which the airflow preferentially occurs. See, for example, Wilson et al. (1995), Rodriguez-Maroto et al. (1995), and the discussion on rate-limited mass transfer in {I}.

Active extraction becomes uneconomical if tailing prolongs extraction, or if buried wastes slowly release volatile contaminants for an indefinite future, or if the contamination has spread to a large area. In these cases, it is attractive to employ passive extraction. If one-way flow is desired, a check valve may be used.

The application of passive SVE has been hampered by an absence of quantitative design techniques for estimating ventilation rates. Only a few authors report mathematical methods for predicting the flow in open wells. Thorstenson et al. (1998) note extensive measurements of the flow in open boreholes due to wind, barometric, and thermal–topographic effects in fractured rock at Yucca Mountain, but do not present general techniques for prediction of flow. Rossabi and Falta (2002) treat a single, homogeneous stratigraphic layer with a one-dimensional impulse–response function analysis of both the vertical penetration of pressure variations from ground surface and the radial flow at a screened interval of a well. Presumably, this technique could be extended to a stratigraphy consisting of multiple layers. Ellerd et al. (1999) treat the advective flow and contaminant transport with two-dimensional numerical simulation of the time history of flow. Simulation enables detailed evaluation of a particular situation, but it does not reveal the general relationships among parameters that may

be obtained from an algebraic solution. Therefore, this paper presents an algebraic model of barometric flow in an open well or borehole, applicable to a variety of situations.

2. Comparison of analytical methods

An earlier report {II} used harmonic analysis to interpret measurements of the vertical penetration of barometric variations in horizontal strata. This article documents measurements of barometric flow in an open well in that same strata, together with harmonic analysis of radial flow in a cylindrical geometry. These plane and cylindrical harmonic solutions are mathematically equivalent to the impulse–response solutions of Rossabi and Falta (2002), but are quite different in physical interpretation and practical application. The impulse technique describes barometric pressure history as a succession of step changes, and solves for the propagation of each step change, either vertically from ground surface or radially from an open borehole. In contrast, the harmonic method describes barometric pressure history as a set of endless sinusoidal cycles, and solves for the propagation of each frequency component.

Calculation of flow by either mathematical technique requires that the investigator have barometric pressure data for a typical span of time. Synoptic weather events, particularly during the winter, typically occur at intervals of 5 days or more. To provide a pressure spectrum for harmonic analysis, the data should contain several representative cycles. Therefore, for harmonic analysis, a barometric pressure history should be obtained for at least 32 days, and preferably for 64 days or more. For the design of a passive venting system, it may not be necessary to measure the pressure history on site, because pressure data are often available from local weather stations or archives such as the National Climatic Data Center (2001).

For use of either mathematical technique, it is necessary either to measure the vertical and horizontal permeability and the porosity of each stratum, or to estimate these values, or to obtain values by fitting a model to measured pressure data, as done by Weeks (1978), Ellerd et al. (1999), and Rossabi and Falta (2002). In {II}, the vertical permeability of each stratum was estimated by fitting the measured penetration of barometric variations to the harmonic model of layered formations. Values of the horizontal permeability used here were measured by air extraction with a straddle packer apparatus, and were reported in {II}.

3. The experimental apparatus and procedures

3.1. The experimental situation

Experimental data were obtained at Well 1006, located on a narrow finger mesa near Los Alamos, NM, USA, at a site where an organic vapor plume remains from previous burial of chemicals. The stratigraphy of the mesa and a description of several boreholes, including Well 1006, were presented in {II}. Well 1006 was originally completed as a

monitoring well with an inflated membrane liner. For the experiment reported here, the liner was removed and the borehole was vented to the atmosphere while the flow rate, the concentration of vapors (including water) in the influent and effluent gas, barometric pressure, and subsurface pressures at several other monitoring wells were monitored. During this test, all other boreholes in the vicinity were configured as monitoring wells or otherwise sealed from the atmosphere.

Well 1006 was drilled by auger at a 65° dip angle to a total length of 97 m. The borehole diameter is approximately 20 cm, varying slightly with position along the borehole. A surface casing extends to 9 m length below ground surface. The remainder of the borehole is uncased. Although Well 1006 was reamed prior to the extraction test, approximately 7 m of rubble may have remained in the bottom of the well.

3.2. Instrument design

Fig. 2 is a diagram of the flow measuring apparatus, which was designed to present insignificant impedance to the flow. The borehole inhaled and exhaled through a 101-mm diameter plastic measuring pipe, 9 m long, suspended in the top of the borehole. Air velocity was sensed by two thermal anemometers located midway between the ends of the pipe. The length of pipe between either end and the anemometers was equivalent to 45 diameters of pipe. This length was intended to establish well-developed flow from either direction at the location of the anemometers. The radial profile of velocity in the pipe was therefore expected to be the same with either downward or upward flow, enabling the calibration of the anemometers to be independent of flow direction. To avoid accumulation of ice condensed from water vapor exhaled during the winter, the measuring pipe was suspended in the borehole, where most of the pipe's length would be below the freezing depth. The pipe was girdled by three metal disks (two shown), intended to retard vertical convection from the borehole into the annular space between the measuring pipe and the well casing. The annular space above the top disk was filled with fiberglass insulation. Although the fiberglass was wetted by condensed water vapor diffusing upwards from the borehole, it provided sufficient insulation from the surrounding frozen soil that ice accumulation was not noticed in the pipe during the winter. The top of the well was shielded from the wind by a fabric tent, shown in Fig. 2.

The measuring pipe was held off-center in the well by several radial support skids (one shown in Fig. 2). The off-center location provided sufficient radial space for two redundant, omnidirectional anemometers (Model 8475, TSI, St. Paul, MN, USA). Electronic units for the anemometers were mounted in a temperature-controlled box external to the well. The sensing elements of the anemometers were located at a radius equal to 70% of the inside radius of the pipe. At this radius, the local velocity is nearly equal to the average velocity during either laminar or turbulent flow, thereby in principle rendering the calibration of the flowmeter insensitive to the laminar–turbulent transition.

A Campbell Scientific Model CS500 temperature and humidity probe was located just below the bottom of the measuring pipe (Campbell Scientific, Logan, UT 84321, USA). An identical probe was located in the atmosphere near the well. Comparison of water vapor density in the borehole with the density in the ambient atmosphere indicated the

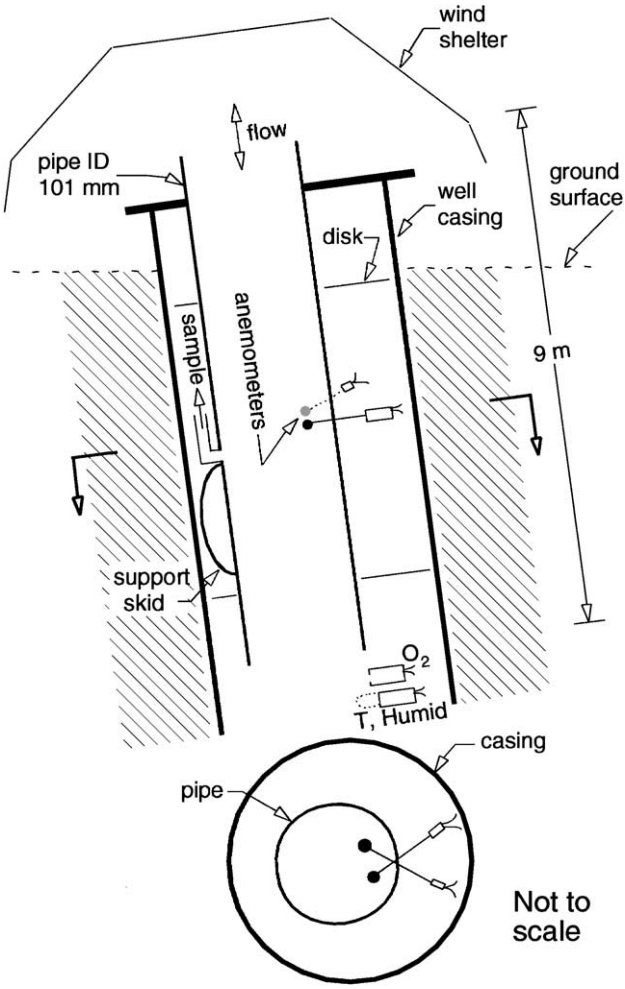

Fig. 2. Schematic cross-section of the flow measuring apparatus suspended in the top of the borehole. Oxygen, temperature, and humidity sensors were suspended beneath the measuring pipe.

direction of flow and enabled inference of the moisture removal. An oxygen sensor was located below the measuring pipe.

Prior to insertion in the well, the measuring pipe was suspended vertically in the laboratory for calibration, with a 200-l drum attached at the lower end and the top end open to the room. A blower forced air into or out of the drum. Thus, for downward flow, air could freely enter at the top of the pipe, as it would in the field installation. For upward flow from the bottom of the pipe, the drum was expected to dissipate the jet from the blower, allowing flow as it would occur in the well. A mass flowmeter was connected between the blower and the drum. The calibrations for upward and downward flow were within approximately 10% of each other, but were not identical.

3.3. Field test procedures

As described in {II}, if data are recorded at intervals of $1/2^p$ day for a window of 2^q days, in which p and q are integers, then the fast Fourier transform will include periods of exactly 1 day and harmonics of 1 day. It was desired that the 1-day atmospheric S-tide and its harmonics be uniquely resolved when the time series pressure data were transformed to frequency components. Accordingly, the atmospheric pressure and all sensors of the flow apparatus were recorded at 45-min intervals, providing 2^5 intervals per day. To avoid the effects of short transients, flow and pressure readings were acquired at approximately 5-min intervals and the results averaged for each 45-min record. (Because frequency components with periods less than 4 h contribute little to the flow, it would have been sufficient in this test to acquire data at intervals of 90 min or 3 h.) At 3-h intervals, a separate automatic apparatus sampled gas from the port in the middle of the measuring pipe shown in Fig. 2, and from several ports of various monitoring wells. Within the automatic apparatus, the gas samples passed to Bruel and Kjaer Model 1302 nondispersive infrared analyzer, which measured concentrations of various organic vapors and CO_2. (The instrument is currently marketed by Innova AirTech Instruments, Energivej 30, DK-2750 Ballerup, Denmark). The infrared analyzer corrects for the interference of the spectrum of one analyte with another. However, because gas extracted from the vadose zone is nearly saturated with water, the correction for the interference of water may be imperfect, and the concentrations reported by the gas sampling apparatus are regarded as qualitative indicators, not as calibrated measurements. Other gas-sampling activities showed that the results from the infrared analyzer were usually close to the results of laboratory analyses. Data and analysis regarding the extraction of vapors will be presented in a separate report.

3.4. Data treatment

All data were reduced to engineering units by a computer program in which flow direction was determined to be out of the ground (negative direction) when the absolute humidity in the measuring pipe was greater than the ambient absolute humidity. In the few instances of rainy weather, when the ambient absolute humidity was indistinguishable from that of the pore gas, the flow direction was established by inspection of the trend in barometric pressure and recent flow history. Either 32- or 64-day windows of data were selected for analysis. As described in {II}, the windows were selected so that the barometric history for two days prior to the window closely matched the history during the last 2 days of the window. The barometric pressure data were transformed to the frequency domain, and the resulting spectra of amplitude and phase were used in calculating a theoretical value of the flow rate at each 45-min interval.

4. Harmonic model of flow

An outline of the harmonic analysis of a freely breathing borehole will be presented here. Notation is defined at the end of this paper and details are presented in Appendix A.

As explained in {II}, the propagation of a small pressure change in a porous medium is described by the diffusion equation:

$$\nabla^2 P(x,t) = \frac{\mu\theta}{kP_0}\frac{\partial P(x,t)}{\partial t}, \tag{1}$$

in which the term $(kP_0/\mu\theta)$ is the pressure diffusivity.

The atmospheric pressure history at ground surface can be expressed as a Fourier series

$$P(y=0,t) = P_{00} + \sum_n P_{n0}\mathrm{e}^{i(\omega_n t+\varphi_{n0})} = P_{00} + \sum_n \boldsymbol{P}_{n0}\mathrm{e}^{i\omega_n t}, \tag{2}$$

in which P_{00} is the average pressure, P_{n0} is the amplitude at zero depth of the frequency component having angular frequency ω_n and phase at zero depth ϕ_{n0}. In the equations, bold type indicates complex quantities with implicit amplitude and phase.

4.1. Plane vertical flow

A single frequency component of pressure propagates downward with depth y in a uniform infinitely deep earth as

$$\boldsymbol{P}_n(y) = \boldsymbol{P}_{n0}\mathrm{e}^{-\beta_n y}\mathrm{e}^{-i\beta_n y}, \tag{3}$$

in which

$$\beta_n = \sqrt{\frac{\omega_n\mu\theta}{2kP_{00}}}. \tag{4}$$

In plane propagation, the local face velocity (so-called "darcy velocity," equivalent to volume flow rate per unit area) of the gas for one component is given by

$$\boldsymbol{V}_n(y) = \sqrt{2}\frac{k}{\mu}\beta_n\boldsymbol{P}_n(y)\mathrm{e}^{i\pi/4}. \tag{5}$$

Note in Eq. (5) that, for any frequency component, the phase of velocity at any location leads the phase of local pressure by 45°.

4.2. Radial flow

Wigley (1967) applied harmonic analysis in cylindrical geometry to explain the breathing of caves. The cylindrical solution in terms of Bessel functions presented in this section is mathematically equivalent to Wigley's solution. Appendix A of this paper presents simple, approximate expressions for the amplitude and phase of the cylindrical solution, so that the reader who wishes to use this method does not need to evaluate the complex Bessel functions, or the corresponding Kelvin functions, for himself.

As an approximation, radial flow is calculated according to the local rock properties along the borehole, although the borehole is not perfectly perpendicular to the horizontal stratigraphy. In effect, the calculation proceeds as though the permeability is constant in a

radial direction from the borehole, even though a radial vector may pass from one horizontal stratum into another. This approximation is valid except for those instances in which the permeability changes greatly at a contact, and a stratum thickness is smaller than the penetration length, $1/\beta$.

Corresponding to Eq. (3) for plane geometry, the solution in cylindrical geometry of infinite extent, at radius r from a borehole of radius r_b, is (Carslaw and Jaeger, 1959)

$$\boldsymbol{P}_n(r) = \boldsymbol{P}_n(r_b)\frac{\mathbf{K}_0(\sqrt{2i}\beta_n r)}{\mathbf{K}_0(\sqrt{2i}\beta_n r_b)}. \tag{6}$$

Corresponding to Eq. (5) for plane flow, the velocity in cylindrical geometry is given by

$$\boldsymbol{V}_n(r) = \sqrt{2}\frac{k}{\mu}\beta_n \boldsymbol{P}_n(r_b)\mathrm{e}^{i\pi/4}\frac{\mathbf{K}_1(\sqrt{2i}\beta_n r)}{\mathbf{K}_0(\sqrt{2i}\beta_n r_b)}. \tag{7}$$

The radial volume flow rate per unit length of borehole is the velocity of Eq. (7) at radius r_b multiplied by the area of borehole wall per unit length, $2\pi r_b$. The borehole radius and soil properties may vary with depth. Accordingly, for a segment of borehole designated by j, and for a frequency designated by n, we define a local complex admittance as the volume flow rate per unit length, per unit variation of atmospheric pressure:

$$\boldsymbol{A}_{nj} = 2\pi\frac{k}{\mu}\sqrt{2}\beta_{nj} r_{bj}\mathrm{e}^{i\pi/4}\frac{\mathbf{K}_1(\sqrt{2i}\beta_{nj} r_{bj})}{\mathbf{K}_0(\sqrt{2i}\beta_{nj} r_{bj})}. \tag{8}$$

The volume flow rate of one frequency component at any segment of the borehole is

$$\boldsymbol{Q}_{nj} = L_j \boldsymbol{A}_{nj}\boldsymbol{P}_{n0}. \tag{9}$$

The admittance of a segment can be expressed explicitly in terms of an amplitude and phase,

$$\boldsymbol{A}_{nj} = A_{nj}\mathrm{e}^{i\Phi_{nj}}, \tag{10}$$

which enables the volume flow rate of the segment to be expressed as a function of real numbers only, if desired:

$$Q_{nj}(t) = \mathrm{Re}(\boldsymbol{Q}_{nj}\mathrm{e}^{i\omega_n t}) = L_j A_{nj} P_{n0}\cos(\omega_n t + \varphi_{n0} + \Phi_{nj}). \tag{9a}$$

4.3. Implications of the harmonic model

The magnitude A_{nj} in Eq. (10) describes how the volume flow rate per length of borehole depends on various parameters. As shown in Appendix A, A_{nj} in many circumstances is approximately represented by

$$A_{nj} \approx 2.46\frac{k_j}{\mu}(\sqrt{2}\beta_{nj} r_{bj})^{0.15}. \tag{11}$$

From substitution of Eq. (4) in Eq. (11), it follows that

$$A_{nj} \propto \left(\frac{k_j}{\mu}\right)^{0.925} \omega_n^{0.075} \left(\frac{\theta_j}{P_{00}}\right)^{0.075} r_{\mathrm{b}j}^{0.15}. \tag{12}$$

Eq. (12) presents the sensitivity of the volume flow rate to various design parameters. One-dimensional cylindrical flow is approximately proportional to the horizontal permeability, approximately proportional to the one-sixth power of the borehole radius, and varies little with frequency and porosity. Increasing a borehole radius by a factor of 10 will increase the flow rate by only 41%. The weak frequency dependence of Eq. (12) can be understood as follows. A higher frequency component penetrates less far from the borehole wall than a low frequency component. However, more cycles of high frequency occur per unit time, leading to approximately the same volume flow as would occur with a low frequency of the same amplitude. The greater penetration from the borehole wall provided by low frequencies would presumably make them more beneficial for vapor removal than higher frequencies. However, as shown in the next section, the frequency dependence of flow at any particular depth is complicated by the competing vertical penetration of pressure from ground surface.

5. Two-dimensional propagation of pressure

5.1. Pressure penetrating from ground surface

In Section 4.2, the solution for radial flow implicitly assumed that the borehole wall was the only source of time-varying pressure in the formation. However, as Fig. 1 depicts, barometric cycles also penetrate vertically from ground surface, thereby rendering the radial solution strictly valid only at extreme depths, or beneath a layer of low permeability that effectively stops penetration from ground surface. Near ground surface, the pressure penetrating vertically in the formation is approximately equal to the atmospheric pressure in the borehole, thereby inhibiting radial flow from the borehole. At greater depths, the vertical variations are both attenuated and delayed, so that a temporary high pressure in the borehole may encounter the remnant of a previous low pressure in the formation, allowing an instantaneous value of flow to be larger than predicted by Eq. (9). In infinitely deep uniform ground, a vertically penetrating pressure component at depth y is shifted in phase by the amount $-\beta_n y$ as shown by Eq. (3). If the phase shift is greater than $\pi/2$, the radial flow for that component will be larger than predicted by Eq. (9a). However, such a beneficial phase shift occurs where the pressure amplitude is attenuated by a number smaller than $\mathrm{e}^{-\pi/2}$. Therefore, the beneficial phase shifts occur only where the amplitude in the formation is small, leading to the conclusion that, in uniform earth, the vertical penetration (or "background" pressure) usually acts to oppose radial flow to and from the borehole. The uniform ground serves as a useful conceptual model. However, the vadose zone is rarely either uniform or extremely deep. Therefore, in practice, the vertical penetration of pressure must be either measured or estimated by a mathematical model such as that presented in {II}.

Because flow occurs both at the borehole wall and at ground surface, a two-dimensional solution to Eq. (1) would be required for highly accurate calculations. Two-dimensional diffusion problems with time-varying boundary conditions are often approached with finite element or finite difference numerical simulations. However, a simulation presents only the time history of a particular configuration, while the object of this work is to develop a more general, approximate approach that reveals the general dependence of borehole flow on parameters such as the borehole radius, porosity, and permeability. Section 5.2 presents an intuitive method for combining the vertical and radial propagation of pressure, which is justified by comparison with experiment in Section 6.

5.2. Boundary conditions

The difference between atmospheric pressure in the borehole and pore pressure in the formation determines the radial flow at the borehole wall. Because the flow responds linearly to the pressure gradient, it is tempting to believe that subtracting the background pressure from the pressure in the borehole would, in effect, superimpose the solutions of two linear problems and thereby enable the one-dimensional radial model to yield exactly the correct flow. Fig. 3 demonstrates why subtraction of the background pore pressure (that would exist in the absence of the borehole) does not provide an exact result.

Both the ground surface and the borehole wall are boundaries of the formation with time-dependent atmospheric pressure. Accordingly, Fig. 3a illustrates the actual boundary conditions for which we seek a solution to Eq. (1) throughout the formation. Fig. 3b depicts a sealed boundary at ground surface, for which Eqs. (6)–(10) present the one-dimensional cylindrical solution for radial flow. Fig. 3c depicts an impervious boundary at the borehole wall, for which Eq. (3) presents the corresponding one-dimensional plane solution for the background pressure in a uniform medium, and {II} presents the solution in a medium composed of horizontal layers. In a model, subtracting the calculated background pressure from the borehole pressure would, in effect, combine the boundary

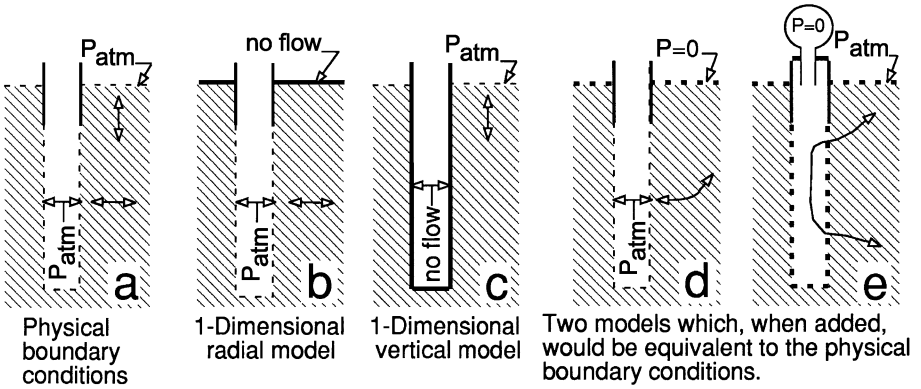

Fig. 3. Diagram illustrating (a) the actual boundary conditions, (b, c) the boundary conditions represented by two one-dimensional harmonic models, and (d, e) the boundary conditions that, if combined, would represent the physical boundary conditions.

conditions of Fig. 3b and c. Those combined conditions are not exactly equivalent to the boundary conditions of Fig. 3a. In contrast, the sum of two solutions representing the boundary conditions depicted by Fig. 3d and e would result in a combined solution representing two free-flowing boundaries, each with atmospheric pressure (literally the sum of atmospheric pressure and zero). This is the actual situation, depicted in Fig. 3a. Fig. 3d illustrates the perturbation to a strictly radial flow by flow to ground surface, and Fig. 3e depicts how the borehole short-circuits vertical flow through the formation. As an approximation, the model uses the radial calculation with an effective pressure in the borehole equal to the atmospheric pressure minus the background pressure. This approximation neglects the two-dimensional flows depicted in Fig. 3d and e.

5.3. The calculational model

In the numerical evaluation of the equations, the slant length of the borehole was represented by 29 segments (designated by the index j), with each segment assigned a permeability and borehole radius according to the straddle packer and caliper measurements made in or near that segment. Segment boundaries corresponded to the contacts of stratigraphic units and subunits noted from the drilling log, or the depth midway between the locations of permeability measurements within a subunit. The porosity, which does not vary widely among the various strata, was assigned to each segment according to laboratory measurements of core samples. The admittance of each segment was calculated according to Eq. (8). In the approximation explained in Section 5.2, the background pressure was subtracted from the atmospheric pressure, so that Eqs. (9) and (9a) became

$$\boldsymbol{Q}_{nj} = L_j \boldsymbol{A}_{nj}(\boldsymbol{P}_{n0} - \boldsymbol{P}_{nj}) \tag{13}$$

and

$$Q_{nj}(t) = L_j A_{nj}[P_{n0}\cos(\omega_n t + \varphi_{n0} + \Phi_{nj}) - P_{nj}\cos(\omega_n t + \varphi_{nj} + \Phi_{nj})], \tag{13a}$$

in which $\mathbf{P}_{nj}$ is the complex background pressure of the nth frequency component at the depth of the jth segment of the borehole. Flow in the entire borehole was calculated by a sum over frequency components of the sum of contributions of each segment at each frequency:

$$Q = \sum_n \sum_j Q_{nj}; \quad Q(t) = \sum_n \sum_j Q_{nj}(t). \tag{14}$$

Fractured strata and a ventilated basalt layer beneath the borehole caused unusual variation of the background pressure, which was known as a function of frequency and depth from earlier measurements at this borehole presented in {II}. For computational convenience, the known magnitude and phase of background pressure were represented as analytic functions of frequency and slant depth along the borehole. However, in a general design tool for passive SVE, the background pressure could be calculated by the equations for layered media presented in {II}.

6. Predicted and measured flow

6.1. Presentation of data

Fig. 4 shows the atmospheric pressure as a function of time for a 64-day summer window and a 32-day autumnal window of data. These windows were selected to minimize the influence of residual subsurface pressures as explained in the appendix of {II}. As shown by Fig. 4, the pressure during the summer is dominated by diurnal

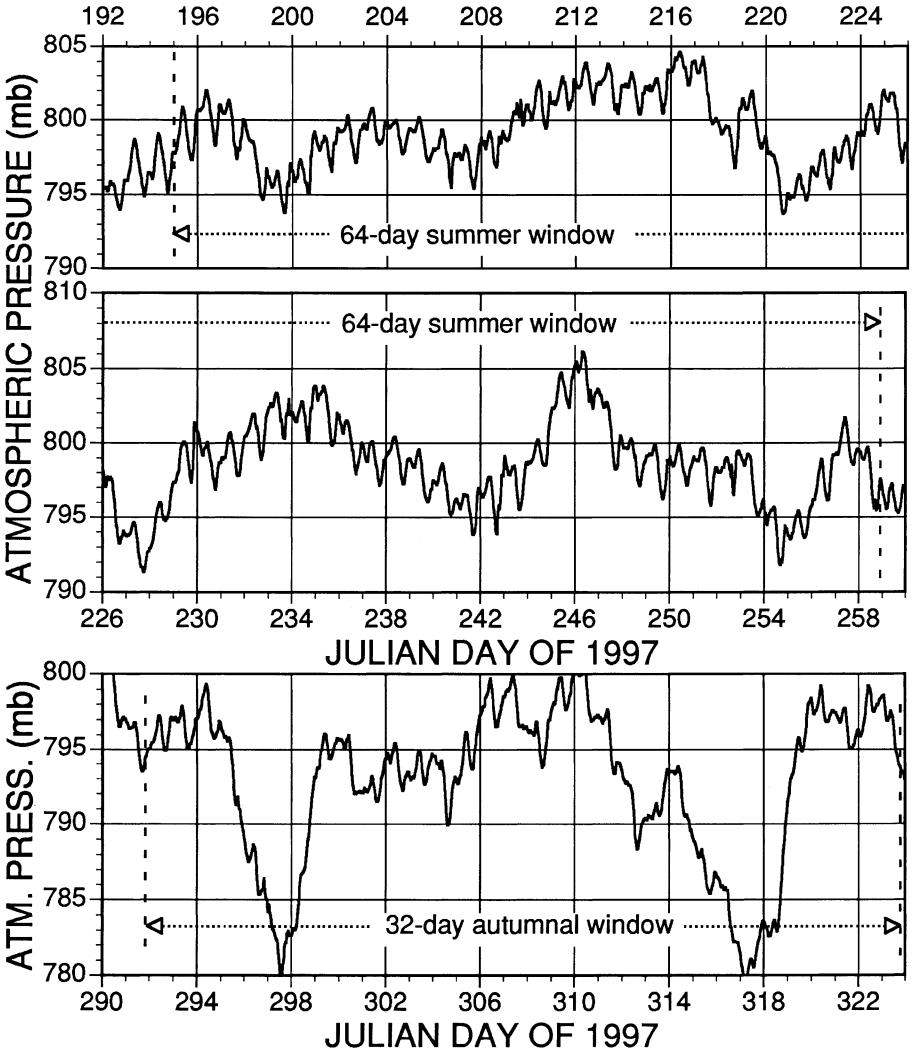

Fig. 4. Atmospheric pressure versus time for the two windows of data that were transformed to the frequency domain.

variations with occasional low pressure events. During autumn and winter, the pressure is dominated by low-pressure storms at intervals of 5 to 20 days. Fig. 5 shows the amplitude, P_{n0}, of the atmospheric pressure spectrum as a function of period for each of the windows. The data are plotted as points with connection to the horizontal axis to emphasize that periodic sampling generates a discrete spectrum of individual frequencies (or periods)—not a continuous curve. Doubling the length of a window would generate twice the number of points in a given interval of periods, but the components of synoptic variations would have smaller amplitudes. In both windows of Fig. 5, the harmonics of the diurnal S-tides at 1, 1/2, 1/3 day, etc. are unique and appear prominently.

Fig. 6 displays typical data, including the oxygen concentration at the bottom of the measuring pipe, the water vapor density in the atmosphere and in the borehole, the flow rate, and the atmospheric pressure. Flow rates greater than zero indicate flow into the ground, as occurs with increasing atmospheric pressure. The two redundant anemometers were labeled "G" and "B," respectively. Anemometer B was damaged during insertion of the apparatus in the borehole and was replaced in the field. Consequently, it did not have a calibration in the laboratory. In the data, Anemometer B usually agrees with Anemometer

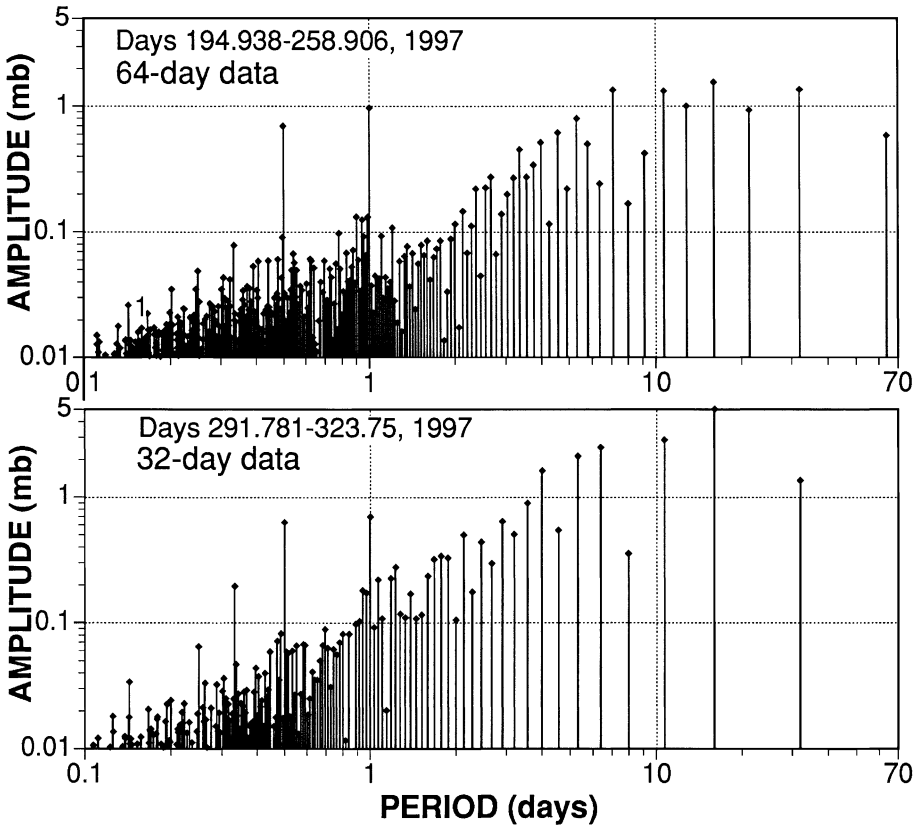

Fig. 5. Amplitude versus period for the components of atmospheric pressure data in the two windows.

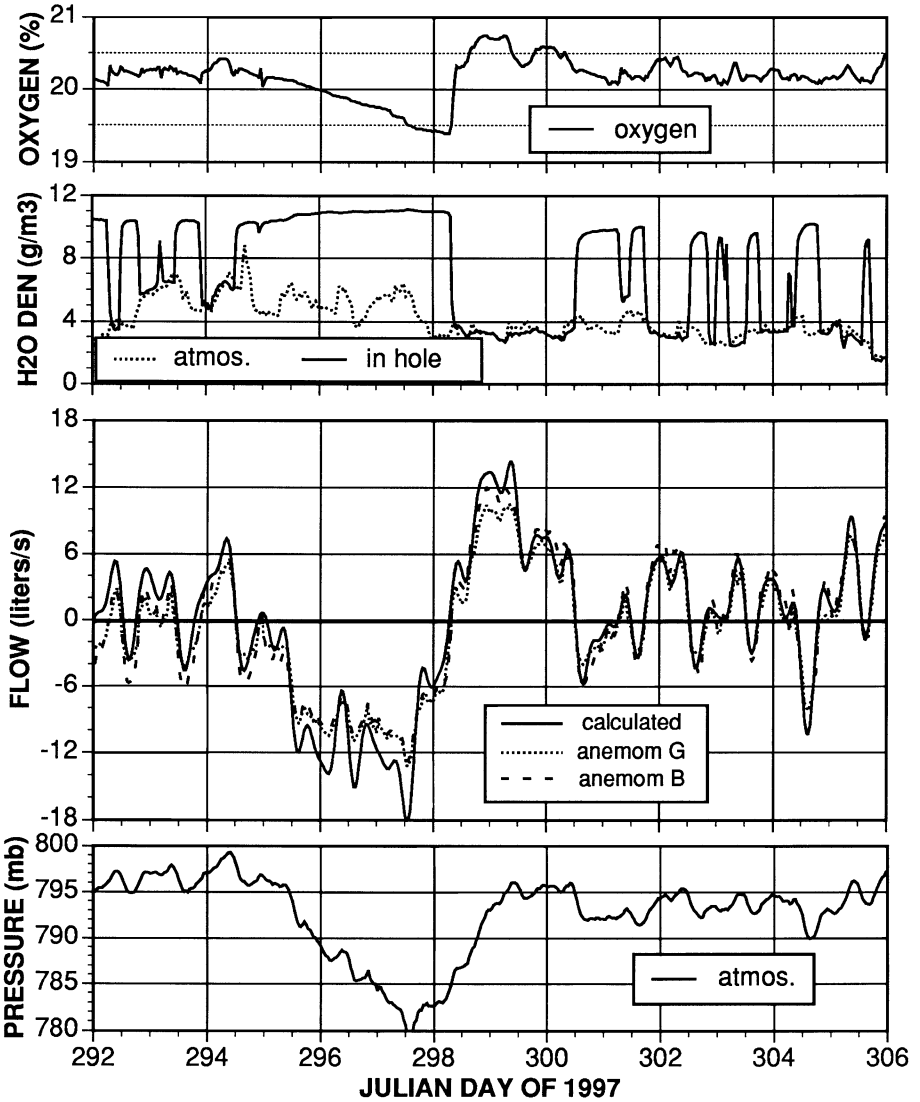

Fig. 6. Typical data acquired at 45-min intervals, illustrating how the concentrations of oxygen and water vapor reveal direction of flow.

G, except at times of peak flow. The disagreement between the anemometers is not consistent and is therefore not due to an uncertain calibration. This varying disagreement is not understood, but could possibly be caused by irregular circumferential variation of flow within the measuring pipe. Data of Anemometer B are included in Fig. 6 to illustrate the uncertainty in the flow measurements.

The general agreement of calculated and measured flow rates illustrated in Fig. 6 exists throughout both data windows. The calculated values generally agree with the measured

values, except that the calculation exaggerates the peaks, whether those peaks occur at small or large flow rates. It was suspected that small-amplitude, high frequency components of pressure or flow were not measured correctly, but eliminating all components with periods less than 0.3 days from the calculation made little difference. The selective disagreement of the two anemometers at peak flows leaves the suspicion that the calculated flow may be more representative of the actual behavior. Winds often occur at times of rapid barometric change associated with peak flows, and it is possible that the wind perturbed the pressure at the opening of the measuring pipe, despite the wind shelter. As explained above, the anemometers were deliberately located off-center in the measuring pipe to render the measurements insensitive to the laminar–turbulent transition in well-developed flow. The measured values would have a varying error if the profile of velocity versus radius in the measuring pipe were somehow dependent upon recent flow history, as might occur if the flow were not well developed during times of rapid fluctuation.

6.2. Measured and calculated admittance

The admittance of the entire borehole at a given frequency is defined as the complex ratio of the volumetric flow component to the atmospheric pressure component at that frequency. Because the background pressure must be subtracted as it varies with depth, the admittance of the entire borehole at a particular frequency cannot be calculated as a sum (over the depth index j) of the complex (admittance × length) products of the individual segments. Instead, the calculated admittance of the entire borehole at frequency n must be obtained from the calculated flow at that frequency, as

$$\boldsymbol{A}_n = \frac{1}{\boldsymbol{P}_{n0}} \sum_j \boldsymbol{Q}_{nj} = \frac{1}{\boldsymbol{P}_{n0}} \sum_j \boldsymbol{A}_{nj} (\boldsymbol{P}_{n0} - \boldsymbol{P}_{nj}) L_j. \tag{15}$$

The measured admittance of the entire borehole is the ratio of the complex frequency component of the measured flow rate to the complex frequency component of atmospheric pressure. Because of the variation of background pressure with depth, the admittance of the borehole depends upon the pressure spectrum. However, the spectrum does not change greatly from season to season, so the admittance is not expected to vary greatly from one season to another.

Fig. 7 presents the measured and calculated amplitudes and phases of the admittance of the entire borehole for the two data windows. As expected, the amplitude and phase of the calculated admittance changed very little between the two windows, and may be regarded as a property of the borehole for practical purposes. In Fig. 7, the magnitude of the admittance varies approximately as the period raised to the -0.44 power (or as frequency to the $+0.44$ power), in contrast to the very weak frequency dependence expressed in Eq. (12). Most of the frequency dependence of flow in the borehole is due to the attenuation of background pressure in the formation, where higher frequencies are preferentially attenuated.

In Fig. 7, the 64-day data scatter less and are closer to the calculated curves than the 32-day data, as may be expected both because the 64-day window contains more data, and

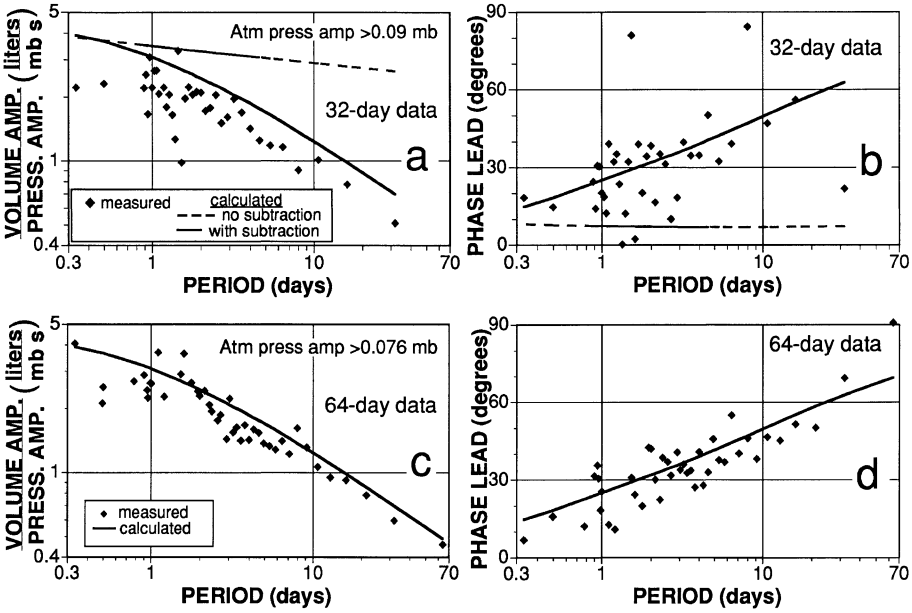

Fig. 7. Amplitude and phase of the admittance of the entire borehole as a function of period, as calculated and as measured. Points are not shown in the 32- and 64-day windows for which the atmospheric pressure amplitude was less than 0.09 or 0.076 mb, respectively, because the corresponding components of flow were beyond the resolution of the apparatus. The dashed curves in (a) and (b) represent illustrative calculations in which the background pore pressure was not subtracted.

because the 64-day window did not contain the dramatic pressure excursions due to storms, which have long periods and are less well represented by the transform of a window of limited width. The dashed curves in Fig. 7a and b represent the calculated admittance when background pressure is not subtracted at each depth interval of the borehole. The dashed curves are far from the data while the solid curves are close to the data, indicating that the subtraction procedure represents a valid approximation. The dashed curves illustrate the weak dependence on frequency exemplified by Eq. (12).

The solid curves of Fig. 7 represent a calculation from first principles without any factors adjusted to fit the data. The agreement with measured data suggests that, for design of passive SVE systems, the barometric flow in open boreholes can be predicted using only the hydrogeologic properties of the formation and a spectrum derived from a typical history of local barometric pressure. At the site of this experimental work, the vertical penetration of barometric pressure is unusual, and the subtraction was based on a careful representation of measured data. However, the calculated flow changed very little when a much more approximate representation of the background pressure was used. Consequently, at sites with more uniform subsurface properties, adequate results may be expected without measuring the vertical penetration, but using a calculated estimate instead.

Table 1
One-way flow into or out of the borehole

	32-day measured	32-day calculated	64-day measured	64-day calculated
Average flow (m^3/day)	193	242	133	151
Water extracted (kg)	51.4	–	10.6	–

The total volume of air inhaled or exhaled by a borehole is a figure of merit in passive remediation. Table 1 presents the averaged measured and calculated rates of ventilation. The calculated ventilation is 15–25% larger than measured. The combined uncertainty in the measured flow rates and measured permeability values could account for a 25% difference between experiment and theory. Also, the bottom 7 m of the borehole probably contains rubble, including part of the membrane liner described in {II} that was accidentally destroyed during removal. If the rubble sealed the bottom of the borehole, it would reduce the total flow by approximately 10%.

Because the background pressure attenuates with depth, the flow in a borehole will increase with depth if the permeability is constant. To examine flow as a function of depth, the calculated flow in individual segments was summed in three regions of the borehole as documented in Table 2. The sum of the flows in three regions is not exactly equal to the flow in the entire borehole because, depending on the instantaneous profile of background pressure with depth, some segments may be exhaling while others are inhaling at the same time, generating flow between individual regions but not flow to the external atmosphere. To compare the regional flows, Table 2 presents the flow per unit length, divided by the permeability raised to the 0.925 power, which is the approximate dependence of flow on permeability presented in Eq. (12). Table 2 shows that, when adjusted for the permeability, the upper region of the borehole receives about half the flow of the lower region. It must be remembered that the surface casing of this borehole extends to 9 m, so the upper calculational region did not include the length immediately below ground surface where the radial flow would be smallest.

To illustrate the effect of borehole depth, Fig. 8 presents the permeabilities of segments, the magnitude of the admittance per unit length of each segment at two periods, and the admittance per length as scaled to remove the approximate dependence on permeability. For the 1-day component, the scaled admittance becomes approximately constant below

Table 2
Calculated one-way flow in each region[a]

	Region 1	Region 2	Region 3
Slant range (m)	9.1–39.5	39.5–64.3	64.3–97.6
Region length (m)	30.4	24.8	33.3
Average permeability (10^{-12} m^2)	8.0	10.6	2.7
32-day flow (m^3/day)	48.7	70.0	36.6
32-day flow (scaled)	0.42	0.65	1.0
64-day flow (scaled)	0.53	0.72	1.0

[a] One-way flow into or out of the borehole wall. Scaled flow is regional flow per unit length, divided by the permeability raised to the 0.925 power, in relative units.

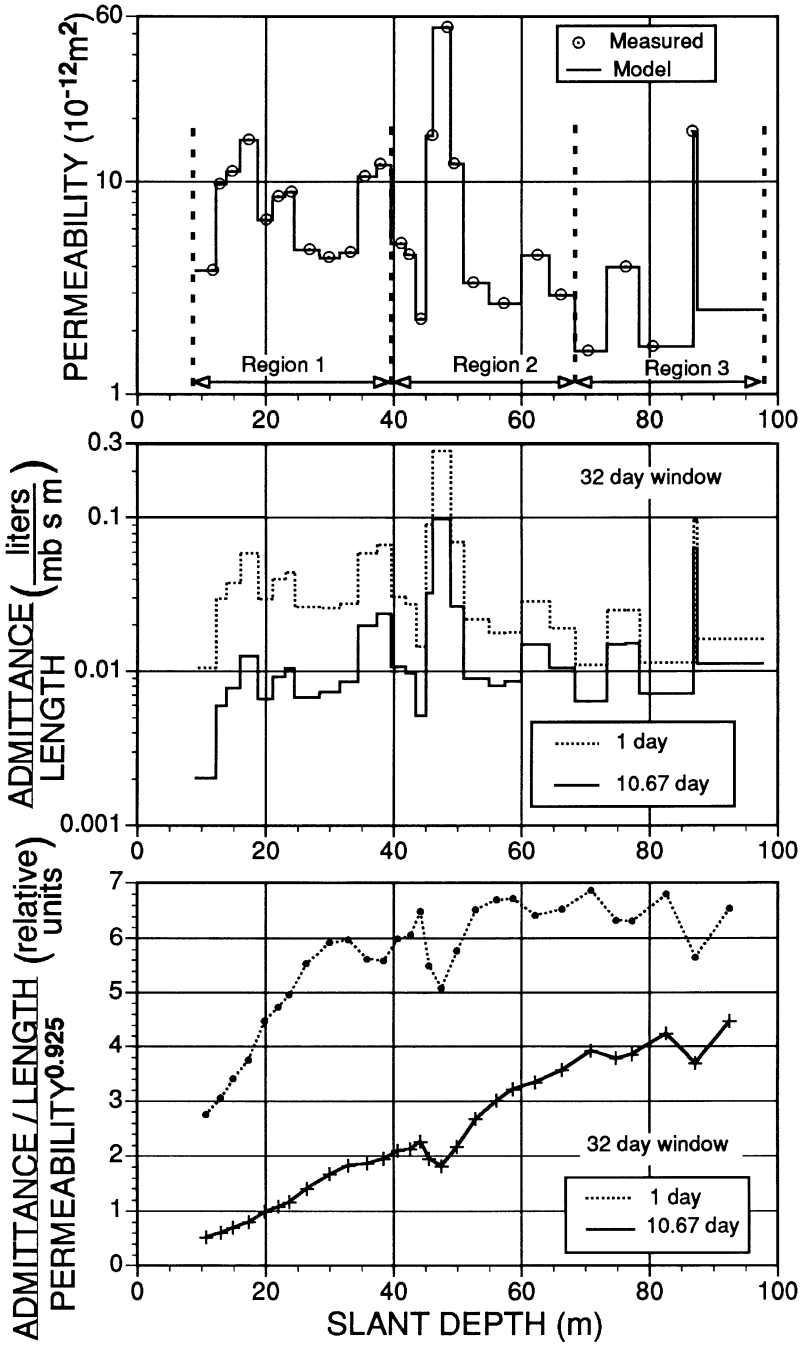

Fig. 8. Permeability, magnitude of admittance per unit length, and scaled admittance per unit length, presented as functions of depth.

50 m of depth because the background pressure has attenuated to insignificance at that depth. However, the amplitude of the 10-day component of pressure is attenuated by only about 50% at 100 m, and the scaled admittance/length increases with depth throughout the borehole.

6.3. A caution in the use of admittance

For passive SVE and bioventing, a figure of merit is the average volume of air inhaled and exhaled per unit time. In the harmonic analysis of a linear system, each sinusoidal flow is independent of the others. It might therefore appear that the investigator could obtain a figure of merit directly by summing the product of borehole admittance amplitude with pressure amplitude over all periods. However, such a process would produce a false result, as explained in Appendix C. It should also be noted that linear methods, such as harmonic analysis and impulse–response theory, cannot be applied to flow governed by a nonlinear element, such as a check valve. One-way flow, as restricted by a check valve, can be represented only by a time-dependent simulation.

7. Conclusions

(1) Harmonic analysis has successfully predicted the time-dependent flow induced in an open borehole by barometric pressure fluctuations. For design of a passive remediation system, the method can be applied using a typical barometric pressure history, the horizontal permeability as a function of depth along the borehole, and the subsurface pressure variation produced by the vertical penetration of barometric cycles from ground surface. The vertical penetration can be estimated with the harmonic method presented in {II}.

(2) At each depth, the approximate flow can be calculated using the atmospheric pressure minus the pore pressure in the undisturbed formation far from the borehole. The flow calculated with this approximation generally differed from the measured flow by less than 25%, which is within the combined uncertainties of the flow rate measurement, the in situ permeability measurement, and the possible effect of rubble in the borehole.

(3) The harmonic model reveals the dependence of the flow rate on borehole parameters. The flow rate is approximately proportional to the permeability raised to the 0.925 power, to the porosity raised to the 0.075 power, and to the borehole radius raised to the 0.15 power. Thus, the flow rate is nearly proportional to the permeability, but increases very weakly with the porosity and borehole radius.

Notation

$\mathbf{A}$	Complex admittance
i	Square root of -1
j	Subscript denoting a segment of depth along the borehole
$\mathbf{K}_0$, $\mathbf{K}_1$	Modified Bessel functions of a complex argument
k	Permeability
L	Length of a segment of the borehole

N_0, N_1	Magnitude of the corresponding Bessel function
n	Subscript denoting a frequency component
P	Pressure
$\mathbf{P}$	Small variation of pressure, expressed as a complex number
P_{00}	Time-averaged atmospheric pressure, approximately 80,000 Pa at the site
Q	Volume flow rate
$\mathbf{Q}$	Volume flow rate, expressed as a complex number
r	Radius
r_b	Radius of borehole
t	Time
$\mathbf{V}$	Face velocity of the pore gas
W	Width of a data window, in this case, 32 or 64 days
x	Any space coordinate
y	Vertical depth below ground surface
z	$(2)^{1/2}\beta r_b$
β	$(\omega\mu\theta/2kP_{00})^{1/2}$, exponential factor for pressure attenuation
θ	Porosity
μ	Viscosity of air
Φ	Phase of the admittance of a borehole segment
ϕ	Phase, or phase difference of a frequency component or Bessel function
ψ_n	Phase of a frequency component of volume flow rate of the entire borehole
ω	Angular frequency

Bold characters indicate complex numbers or functions.

Acknowledgements

The experimental test was conducted as part of an investigation at the Los Alamos National Laboratory, whose support of the test is gratefully acknowledged. Although the analysis and interpretation presented here are the private activity of the author, the experimental test was a team effort in which R. Gilkeson supervised the drilling, Wm. Lowry supervised the permeability measurements, S. Limback constructed the flow measuring apparatus, and K. Kisiel conducted data acquisition.

Appendix A. Evaluation of equations

In this appendix, we evaluate the radial flow at one particular depth and at one frequency, omitting the subscripts j and n.

Replacing $e^{i\pi/4}$ by $(i)^{1/2}$ in Eq. (8), we see that the complex admittance is proportional to the ratio of two Bessel functions of the same complex argument:

$$\boldsymbol{A} = 2\pi\frac{k}{\mu}\sqrt{2i}\beta r_b\frac{\mathbf{K}_1(\sqrt{2i}\beta r_b)}{\mathbf{K}_0(\sqrt{2i}\beta r_b}. \tag{A1}$$

If the argument is expressed in terms of the real number z as

$$z \equiv \sqrt{2}\beta r_b, \tag{A2}$$

then the Bessel functions can be written explicitly in terms of amplitudes and phases:

$$\boldsymbol{K}_0(\sqrt{i}z) = N_0 e^{i\varphi_0}; \quad \boldsymbol{K}_1(\sqrt{i}z) = N_1 e^{i\varphi_1}, \tag{A3}$$

so that Eq. (A1) becomes

$$\boldsymbol{A} = 2\pi \frac{k}{\mu} z \frac{N_1(z) e^{i\varphi_1(z)}}{N_0(z) e^{i\varphi_0(z)}} e^{i\pi/4}. \tag{A4}$$

McLachlan (1961) presents series approximations for the real functions N_0, N_1, ϕ_0, and ϕ_1, permitting easy evaluation of N_1/N_0 and $(\phi_1 - \phi_0 + \pi/4)$ as functions of z. (Readers should be aware that McLachlan's expression for ϕ_1 beneath Table 30 on page 230 apparently contains typographical errors.) For computation with $0.001 < z < 1$, the magnitude of N_1/N_0, can be represented by

$$\frac{N_1(z)}{N_0(z)} \approx 1 + \frac{0.3922}{z^{0.8511}}. \tag{A5}$$

For $z < 0.2$, the phase (in degrees) of Eq. (A4) can be represented by

$$\phi_1 - \phi_0 + 45^\circ \approx 29.87 + 15.50 L_{10}(z) + 2.612[L_{10}(z)]^2, \tag{A6}$$

in which L_{10} represents the logarithm to the base 10. At large values of r_b, the phase approaches 45°, as is the case for the plane wave penetration of Eq. (5).

For most situations where passive vapor extraction is of practical use, $z < 0.01$, and the last term of Eq. (A5) is dominant. Physically, this means that the borehole radius is much less than the penetration depth of a pressure wave at the frequency in question. In that case, combining Eqs. (A4) and (A5) leads to Eq. (11).

Appendix B. Computer program for barometric flow

This appendix presents the key portions of source code for calculating the barometric flow in an open borehole, according to the equations given in Appendix A. In this code, complex quantities are calculated explicitly; therefore the compiler need not support complex variables. Input/output and declarations of storage, as well as any particular items desired by the user, must be added to the code. Such items might include tallies of flow in particular sections of the borehole. The code presented here is for a BASIC compiler, but

can be easily translated to FORTRAN. In this code, variables beginning with I-N do not necessarily indicate integers, as they do in FORTRAN.

In the Fourier transform of pressure data, and in the program shown below, the equation of time is applied to establish all phases relative to local solar midnight on the day in the center of the time window when pressure data were acquired (Duffie and Beckman, 1980). Any other reference time (including zero) might be used, but the time in the harmonic terms of the flow calculation must have the same reference as the time to which the phases of the pressure components are referred.

In the example below, the program uses 96 Fourier components of pressure transformed from 1024 time-sequence data points that were obtained at 45-min intervals during a 32-day window. The window was selected as described in the appendix of {II}. The 96 components have periods of 32, 16, 10.66,. . ., 1/3 days. The 32-day window provides 512 components; however, the components with periods shorter than 1/3 day cause insignificant contributions to flow and are consequently ignored. The example program uses measured values of permeability and borehole radius at each of 29 segments of borehole length to calculate the admittance of each segment according to Eq. (A4). At each period, the complex flows of the segments are added to provide the flow of the entire borehole at that period according to Eq. (15). The program could be modified to accept any set of periodic pressure components or an arbitrary number of segments of borehole length. A specific example is shown here for clarity.

In calculating the admittance at a particular subsurface depth, the program uses an effective pressure at each period. The effective pressure is the complex barometric pressure component minus the complex pore pressure component at the period and depth in question. Amplitudes and phase shifts of pore pressure are obtained from input, not shown. Components of pore pressure may be calculated by the layer model presented in {II}, by Eq. (3) for a homogeneous infinitely deep soil, or by values of pressure amplitude and phase interpolated from measurements at several depths, as illustrated in {II}. Immediately before termination, the example program uses the input barometric pressure components and the calculated admittance to calculate the flow at the same 1024 times when the pressure was measured. However, the program could be altered to calculate the flow at any desired time represented by the variable, TIM#.

B.1. Definitions of important variables and functions

#	Indicates double precision constant or variable.
INT(x)	Largest integer less than or equal to x.
SGN(x)	Function yielding the sign, + or −, of x.
ID	Integer index of a length segment of a borehole (represented by j in the equations).
NP	Integer index of period or frequency component (represented by n in the equations).
IT	Integer index of times at which flow is calculated.
AMPV(ID,NP)	Ratio of pore pressure amplitude at segment ID to atmospheric pressure amplitude, at period NP (input).
PHSV(ID,NP)	Phase shift of pore pressure from atmospheric pressure at segment ID and period NP (radians or degrees) (input).
MU	Viscosity of air at the subsurface temperature (PaS).

P0	average total barometric pressure (Pa).
RB(ID)	Radius of borehole at segment ID (m) (input).
PERMD(ID)	Permeability normal to the borehole axis at segment ID (m^2) (input).
DELM(ID)	Length interval of borehole segment (m) (input).
DIFF(ID)	Pneumatic diffusivity normal to borehole axis at segment ID (m^2/s).
PRAMP(NP)	Amplitude of barometric pressure at period NP (Pa) (input).
PRPH(NP)	Phase of barometric pressure at period NP (radians or degrees) (input).
Z	Defined by Eq. (A2), for a particular segment of borehole as determined by the local radius and permeability.
SUMR	Variable to accumulate the sum over borehole length of the real component of flow rate at one period.
SUMI	Variable to accumulate the sum over borehole length of the imaginary component of flow rate at one period.
VNPN(NP)	Amplitude of flow rate of the entire borehole at period NP.
PHTOT(NP)	Phase of flow rate of the entire borehole at period NP.
AMPT(NP)	Amplitude of the admittance of the entire borehole at period NP.
PHL(NP)	Phase of admittance of the entire borehole at period NP. This is the phase lead of flow ahead of pressure.
JSTART	Julian day and time at first pressure data point.
TSTART	Solar time of day at first pressure data point.
TIM#	Elapsed time from reference for calculation of flow.

B.2. Computational portions of an example program

```
DEF FNLOG10(X) = LOG(X)/LOG(10#) 'define fctn log base 10
DEF FNN1N0(Z) = 1 + .3921939#/(Z^.8511157#)  'define fctn Eq. A5
DEF FNPH(L10Z) = 29.87474 + 15.50295*L10Z + 2.612807*L10Z^2
' define fctn Eq. A6, fit to phase of Eq. A4 in degrees
'   ****input amplitudes and phase shifts of pore pressures
'   at 29 segment locations
'   ****input borehole radius, segment length, porosity, and
'   permeability at 29 segment locations
'   ****input amplitudes and phases of barometric components
'   ****(code not shown)

PI = 3.141593
PI2 = 2*PI
PI# = 3.141592653589795#
PI2# = 2*PI#
MU = .0000178  'viscosity of air, Pa s at 12 deg C.
P0 = 79298.8   'mean atm press, Pa, for Jdays 291-323 1997.
JDAV = 307  'centered Julian day for solar time.
JSTART = 291.7813   'Julian time of first pressure data point
  T1 = JSTART-INT(JSTART)   'standard time after clock midnight
  B = PI2*(JDAV-81)/364
  EOT = (9.87*SIN(2*B) -7.53*COS(B) -1.5*SIN(B)) 'eq time minutes
  SOLMID = (-4.7 + EOT)/1440 'solar midnight at Los Alamos,
(days)
  TSTART = T1 - SOLMID 'time of first data from solar midnite
(days)
```

```
FOR ID = 1 TO 29  'loop through borehole segments
  DIFF(ID) = PERM(ID)*P0/(MU*POR(ID))  'pneumatic diffusivity,
m^2/s
NEXT ID

FOR NP = 1 TO 96 'loop on periods
 PER(NP) = 32/NP     ' period, days
 OMEG#(NP) = PI2#/(PER(NP)*1440*60) ' angular frequency, radian/s
 PRR(NP) = PRAMP(NP)*COS(PRPH(NP))  'real part baro press amp,
clock phase
 PRI(NP) = PRAMP(NP)*SIN(PRPH(NP))  'imaginary part baro press
amp
 NEXT NP
'                ***** OUTER LOOP ON PERIODS  ******
FOR NP = 1 TO 96   'main loop on periods.
SUMR = 0  'initialize sum of real flow components over bore
length

SUMI = 0  'initialize sum of imaginary components over bore
length
'            **** INNER LOOP ON BOREHOLE DEPTH SEGMENTS ****
  FOR ID = 1 TO 29       '29 depth segments of borehole
    SPF = PHSV(ID,NP)  'phase shft of pore pressure, radians
    SPA = PRAMP(NP)*AMPV(ID,NP)  'amp of press component at depth
  PHSOL = PRPH(NP) + SPF 'phase of pore press = phase of atm
press + phase shift of pore press
  EPRR = PRR(NP) - SPA*COS(PHSOL)  'real part of effective press
= atm press-soil press
  EPRI = PRI(NP) - SPA*SIN(PHSOL)  'imag part of effective press
  PRAMPEF= SQR(EPRR^2 + EPRI^2)   'effective pressure amplitude
'  find phase of effective press, avoid small real part
   IF EPRR > 1E-10 THEN   'pos real component
    PHEPR = ATN(EPRI/EPRR)
    ELSEIF EPRR < -1E-10 THEN
    PHEPR = PI + ATN(EPRI/EPRR)
    ELSE         'near zero real component
    PHEPR = .5*PI*SGN(EPRI)    'set phase to pure imaginary
   END IF
'     calculate admittance & flow of one period, one depth
segment
  Z = RB(ID)*SQR(OMEG#(NP)/DIFF(ID))   'z depends on segment
  AMPRAT = PI2*(PERM(ID)/MU)*Z*FNN1N0(Z)  'Eq. A4 amplitude
  L10Z = FNLOG10(Z)   'log10 of Z
  PHASE = FNPH(L10Z)*PI/180   'Eq. A6 converted to radians
  ADMIT = DELM(ID)*AMPRAT 'admittance ampl. of segment (m3/pa s)
'      calculate complex flow for 1 period, 1 depth interval
  VFLO = ADMIT* PRAMPEF 'amplitude of flow, m3/s
  PHFLO = PHEPR + PHASE 'flow phase = ph of eff pr + ph of admit
```

```
REM     sum over segments for flow at one period
  SUMR = SUMR + VFLO*COS(PHFLO)  'add flows of segments
  SUMI = SUMI + VFLO*SIN(PHFLO)
NEXT ID       '**** bottom of loop on borehole segments ****
VNPN(NP) = SQR(SUMR^2 + SUMI^2) 'flow amplitude, entire borehole
IF SUMR > 1E-10 THEN
PHTOT(NP) = ATN(SUMI/SUMR)  'phase of flow, entire borehole
ELSEIF SUMR < -1E-10 THEN
PHTOT(NP) = PI + ATN(SUMI/SUMR)
ELSE
PHTOT(NP) = .5*PI*SGN(SUMI)
END IF
AMPT(NP) = VNPN(NP)/PRAMP(NP) 'admittance at 1 period, for output
PHL(NP) = (PHTOT(NP) - PRPH(NP))*180/PI  'convert to degrees
IF PHL(NP) > 360 THEN
   PHL(NP) = PHL(NP) - 360
   ELSEIF  PHL(NP)< 0 THEN
   PHL(NP) = PHL(NP) + 360 'phase of admittance of entire
borehole
END IF                     ' at 1 period, for output (degrees)
NEXT NP     '**** bottom of loop on periods ****
'        *** calculate flow at a set of times ***
FOR IT = 1 TO 1024   'loop to calculate flow at 1024 times.
 ETIM# = (IT-1)*45*60   'elapsed time since first point (seconds)
 TIM# = TSTART*24*3600 + ETIM# 'elapsed time since solar midnight
 JDAYT(IT) = JSTART + (IT-1)*45/1440
'JDAYT is Julian standard time at IT, calculated for output
(days)
 SUMF# = 0
    FOR NP = 1 TO 96 'sum periodic components of flow at each
time
    SUMF# = SUMF# + VNPN(NP)*COS(OMEG#(NP)*TIM# + PHTOT(NP))
    NEXT NP
 FLOW(IT) = SUMF#  'flow (m3/s) at time 45*IT minutes after start
NEXT IT
'       *** Bottom of IT loop to calculate flow ***
' ** output of admittances and flow values may be inserted here
**
END   ' end of program
```

Appendix C. Calculating the volume inhaled or exhaled

A figure of merit is the total volume of air inhaled or exhaled during a time interval, *W*. It may seem tempting to infer the volume from a sum over frequency of the flow amplitudes at individual frequencies. However, to obtain the inhaled or exhaled volume,

one must first calculate the total flow as a function of time, and then integrate the flow in one direction, as explained below.

Any transformed time window of duration W would include an integral number, n, of cycles of the nth frequency component. That is, for Fourier component n,

$$\omega_n = \frac{2\pi n}{W}. \tag{C1}$$

The instantaneous flow rate of this component is of the form

$$Q_n \cos(\omega_n t + \psi_n) = \mathrm{Re}\{\boldsymbol{A}_n \boldsymbol{P}_{n0} \mathrm{e}^{i\omega_n t}\}. \tag{C2}$$

For this single component, the volume inhaled or exhaled by the borehole during time interval W would be

$$\int_0^W [Q_n \cos(\omega_n t + \psi_n)]^+ \mathrm{d}t = \frac{WQ_n}{\pi}, \tag{C3}$$

in which the + superscript indicates that contributions to the integral occur only when the integrand is positive. The figure of merit is the total one-way flow generated by all frequency components during the time interval W,

$$\text{Figure of merit} = \int_0^W \left[\sum_n Q_n \cos(\omega_n t + \psi_n)\right]^+ \mathrm{d}t \neq \sum_n \frac{WQ_n}{\pi}. \tag{C4}$$

The figure of merit is not equal to a sum over n of the many individual terms corresponding to Eq. (C3). The individual sinusoidal flow components add to form the total flow at any time. However, the individual components interfere with each other, so that the integrated one-way flow is not the sum of individual one-way integrals.

References

Baehr, A.L., Joss, C.J., 1995. An updated model of induced airflow in the unsaturated zone. Water Resour. Res. 31, 417–421.

Carslaw, H.S., Jaeger, J.C., 1959. Conduction of Heat in Solids, 2nd ed. Clarendon Press, Oxford, p. 193.

DiGiulio, D.C., 1996. Evaluation of soil venting application. In: Boulding, J.R. (Ed.), EPA Environmental Engineering Sourcebook. Ann Arbor Press, Chelsea, MI, USA, pp. 123–132.

Duffie, J.A., Beckman, Wm.A., 1980. Solar Engineering of Thermal Processes. Wiley, New York, p. 9.

Ellerd, M.G., Massmann, J.W., Schwaegler, D.P., Rohay, V.J., 1999. Enhancements for passive vapor extraction: the Hanford study. Ground Water 37, 427–437.

Foor, D.C., Zwick, T.C., Hinchee, R.E., Hoeppel, R.E., Kyburg, C., Bowling, L., 1995. Passive bioventing driven by natural air exchange. In: Hinchee, R.E., Miller, R.N., Johnson, P.C. (Eds.), In Situ Aeration: Air Sparging, Bioventing, and Related Remediation Processes. Battelle Press, Richland, WA, USA, pp. 369–375.

Johnson, P.C., Ettinger, R.A., 1994. Considerations for the design of in situ vapor extraction systems: radius of influence vs. zone of remediation. Ground Water Monit. Rev. 14 (3), 123–128.

Johnson, P.C., Kemblowski, M.W., Colthart, J.D., Byers, D.L., Stanley, C.C., 1990. A practical approach to the design, operation, and monitoring of in situ soil-venting systems. Ground Water Monit. Rev. 10 (2), 159–178.

Massmann, J., Shock, S., Johannesen, L., 2000. Uncertainties in cleanup times for soil vapor extraction. Water Resour. Res. 36, 679–692.

McLachlan, N.W., 1961. Bessel Functions for Engineers, 2nd ed. Clarendon Press, Oxford.

Michaels, P., 1996. In situ soil vapor extraction treatment. In: Boulding, J.R. (Ed.), EPA Environmental Engineering Sourcebook. Ann Arbor Press, Chelsea, MI, USA, pp. 111–122.

National Climatic Data Center, 2001. Data may be ordered through the web site at http://www.ncdc.noaa.gov/.

Neeper, D.A., 2001. A model of oscillatory transport in granular soils, with application to barometric pumping and earth tides. J. Contam. Hydrol. 48, 237–252.

Neeper, D.A., 2002. Investigation of the vadose zone using barometric pressure cycles. J. Contam. Hydrol. 54, 59–80.

Pedersen, T.A., Curtis, J.T., 1991. Soil Vapor Extraction Technology Reference Handbook. U.S. Environmental Protection Agency report EPA/540/2-91/003, available from National Technical Information Service, Springfield, VA 22161, USA.

Rodriguez-Maroto, J.M., Wilson, D.J., Gomez-Lahoz, C., 1995. Soil cleanup by in-situ aeration: XXI. Effects of desorption rates and equilibria on remediation rates. Sep. Sci. Technol. 30, 521–547.

Rossabi, J., Falta, R.W., 2002. Analytical solution for subsurface gas flow to a well induced by surface pressure fluctuations. Ground Water 40, 67–76.

Thorstenson, D.C., Weeks, E.P., Haas, H., Busenberg, E., Plummer, N., Peters, C.A., 1998. Chemistry of unsaturated zone gases sampled in open boreholes at the crest of Yucca Mountain, Nevada: data and basic concepts of chemical and physical processes in the mountain. Water Resour. Res. 34, 1507–1529.

Weeks, E.P., 1978. Field determination of vertical permeability to air in the unsaturated zone. U.S. Geological Survey Professional Paper 1051, available from the Superintendent of Documents, U.S. Government Printing Office, Washington, DC 20402, USA. Stock number 024-001-03092-6.

Wigley, T.M.L., 1967. Non-steady flow through a porous medium and cave breathing. J. Geophys. Res. 72, 3199–3205.

Wilson, D.J., Clarke, A.N., Clarke, J.H., 1988. Soil clean up by in-situ aeration. I. Mathematical modeling. Sep. Sci. Technol. 23, 991–1037.

Wilson, D.J., Rodriguez-Maroto, J.M., Gomez-Lahoz, C., 1995. Soil cleanup by in-situ aeration: XXIII. Effect of air channeling. Sep. Sci. Technol. 30, 2491–2508.